Received 8 June 2019
Revised 28 July 2019
Accepted 30 July 2019

Pseudoplastic natural convection flow and heat transfer in a cylindrical vertical cavity partially filled with a porous layer

Kasra Ayoubi Ayoubloo
Department of Mechanical Engineering, Shahid Chamran University of Ahvaz, Ahvaz, Iran

Mohammad Ghalambaz
Department for Management of Science and Technology Development, Ton Duc Thang University, Ho Chi Minh City, Vietnam and Faculty of Applied Sciences, Ton Duc Thang University, Ho Chi Minh City, Vietnam

Taher Armaghani
Department of Engineering, Mahdishahr Branch, Islamic Azad University, Mahdishahr, Iran

Aminreza Noghrehabadi
Department of Mechanical Engineering, Shahid Chamran University of Ahvaz, Ahvaz, Iran, and

Ali J. Chamkha
Department of Mechanical Engineering, Prince Mohammad Bin Fahd University, Al-Khobar, Saudi Arabiama

Abstract

Purpose – This paper aims to theoritically investigate the free convection flow and heat transfer of a non-Newtonian fluid with pseudoplastic behavior in a cylindrical vertical cavity partially filled with a layer of a porous medium.

Design/methodology/approach – The non-Newtonian behavior of the pseudoplastic liquid is described by using a power-law non-Newtonian model. There is a temperature difference between the internal and external cylinders. The porous layer is attached to the internal cylinder and has a thickness of D. Upper and lower walls of the cavity are well insulated. The governing equations are transformed into a non-dimensional form to generalize the solution. The finite element method is used to solve the governing equations numerically. The results are compared with the literature results in several cases and found in good agreement.

Findings – The influence of the thickness of the porous layer, Rayleigh number and non-Newtonian index on the heat transfer behavior of a non-Newtonian pseudoplastic fluid is addressed. The increase of pseudoplastic behavior and increase of the thickness of the porous layer enhances the heat transfer. By increase of the porous layer from 0.6 to 0.8, the average Nusselt number increased from 0.15 to 0.25. The increase of non-Newtonian effects (decrease of the non-Newtonian power-law index) enhances the heat transfer rate.

Originality/value – The free convection behavior of a pseudoplastic-non-Newtonian fluid in a cylindrical enclosure partially filled by a layer of a porous medium is addressed for the first time.

Keywords Porous layer, Axis symmetric enclosure cylinder, Free convection heat transfer, Pseudoplastic non-Newtonian behaviour

Paper type Research paper

International Journal of Numerical Methods for Heat & Fluid Flow
Vol. 30 No. 3, 2020
pp. 1096-1114

0961-5539
DOI 10.1108/HFF-06-2019-0464

Nomenclature

C = heat capacity ($J/kg.K$);
C_p = specific heat in constant pressure ($J/kg.K$);
L = length of the cylinder;
g = gravity (m/s^2);
k = thermal conductivity ($W/m.K$);
AR = aspect ratio (L/R);
D = the thickness of the porous layer;
P = pressure (Pa);
T = temperature (K);
ΔT = temperature difference;
t = time (s);
L = height (m);
u_r = radial velocity (m/s);
u_z = vertical velocity (m/s);
n = non-Newtonian power-law index;
m = consistency index;
Nu = Nusselt number;
Ra = Rayleigh number;
Pr = Prandtl number;
Da = Darcy number; and
r,z = cylindrical coordinates.

Greek symbols

α = thermal diffusivity (m^2/s);
μ = dynamic Viscosity ($kg/m.s$);
ρ = density (kg/m^3);
ν = kinematic viscosity (m^2/s);
ξ = basis functions;
β = thermal expansion coefficient ($1/K$);
k = permeability;
ε = porosity; and
θ = non-dimensional temperature.

Subscripts

eff = effective;
bf = base fluid;
p = porous layer;
h = hot;
c = cold;
i = inner; and
o = outer.

Superscript

* = non-dimensional.

1. Introduction

In many natural and engineering sciences, behavioral and functional analyses are closely related to heat transfer and momentum of fluids. Besides, many types of fluids, known as non-

Newtonian, cannot be modeled considering the linear relation between shear stress and the rate of strain. In nature and industry, most materials show strange behavior, not predictable by the equation of Newtonian fluids. These materials include suspensions, emulsions, colloidal, glues and blood. Power-law model is considered as one of the most applicable models in estimating the behavior of non-Newtonian fluids (Quarteroni *et al.*, 2000).

Analysis of flow and heat transfer of non-Newtonian fluids in industry and natural porous media, such as blood flowing through living textures, using non-Newtonian polymer in the porous condition to increase oil extraction, and many other items, has crucial importance for engineers and researchers (Chhabra and Richardson, 1999; Siavashi and Vamerzani, 2016).

Various aspects of Newtonian natural convection flows in cavities such as cavities filled with a porous fin (Asl *et al.*, 2019), one layer of a porous medium (Astanina *et al.*, 2019), two (Mehryan *et al.*, 2019) and multiple (Miroshnichenko *et al.*, 2018) layers of porous media, tilted (Sheremet and Pop, 2018) and wavy wall (Alsabery *et al.*, 2019, 2018) porous cavities, and cavities with non-uniform heating (Alsabery *et al.*, 2017a). The natural convection in the porous cavities in the presence of a magnetic field (Dogonchi *et al.*, 2019) and nanoparticles (Sivasankaran *et al.*, 2018) is also addressed. Sheremet (2012) explored the 3D natural convection heat transfer in an inclined cylindrical enclosure. Unsteady conjugate natural convection in cylinders with a layer of porous media (Sheremet and Trifonova, 2014; Sheremet and Trifonova, 2013) were also addressed.

The flow and heat transfer of non-Newtonian fluids have been subject of many previous studies. For example, Kairi and Murthy (2009, 2012), using the boundary layer analysis, investigated the flow and heat transfer of a phase change material over an interface of solid-liquid with the shape of a vertical flat plate. Chamkha *et al.* (2017) explored the mixed convection and entropy generation of a Newtonian magneto hydrodynamic (MHD) nanofluid in a lid-driven cavity.

There are also several recent studies that have analyzed the natural convection heat transfer of non-Newtonian fluids in an enclosure. Kefayati (2016a) investigated the natural convection heat transfer of nanofluid as a non-Newtonian fluid in a porous cavity. Cheng (2009) explored the mixed convection boundary layer of a non-Newtonian fluid over a vertical cone embedded in a porous medium. Kefayati (2016c, 2016b) examined the double-diffusive free convection in an inclined porous cavity with Soret and Dufour effects. In a very recent study, Kefayati (2019) addressed the natural convection of viscoplastic fluids in a porous cavity. Loenko *et al.* (2019) examined the free convection of a power-law fluid in an enclosure containing in the presence of a heat-generating element.

Pishkar *et al.* (2019) addressed the non-Newtonian free convection in a square cavity for pseudoplastic non-Newtonian fluids and dilatant non-Newtonian fluids. The natural convection heat transfer of non-Newtonian fluids in the space between two vertical plates (Biswal *et al.*, 2019), the space between two plates partially filled with a porous medium (Mohebbi *et al.*, 2019), the space between eccentric horizontal Annulus (Harab *et al.*, 2019) and an L-shape cavity (Jahanbakhshi *et al.*, 2018) is investigated. Alsabery *et al.* (2017b, 2015) researched the natural convection heat transfer of a power-law non-Newtonian fluid in a rectangular cavity (Alsabery *et al.*, 2015) and a trapezoidal cavity filled with a porous medium (Alsabery *et al.*, 2017b). The non-Newtonian index of n was in the range of $0.6 \leq n \leq 1.4$. The outcomes show that in the case the trapezoidal cavity, the local Nusselt number is higher for a lower power-law index. The angle of sidewalls of the trapezoidal cavity notably affects the heat transfer. In the case of the rectangular cavity with a layer of a porous medium, it was found that for power-law index less than unity, which represents the pseudoplastic fluids, there is a maximum value of the heat transfer. The increase of

the power-law index significantly decreases the heat transfer rate in the cavity. Raizah *et al.* (2018) explored the free convection heat transfer of a non-Newtonian fluid with the power-law index n from 0.4 to 1 in a porous cavity. The outcomes show that an increase in the power-index n decreases the rate of heat transfer.

As seen, the analysis of free convection flow and heat transfer has been the subject of some recent studies. However, in all of these mentioned studies (Pishkar *et al.*, 2019; Biswal *et al.*, 2019; Mohebbi *et al.*, 2019; Harab *et al.*, 2019; Jahanbakhshi *et al.*, 2018; Alsabery *et al.*, 2017b, Alsabery *et al.*, 2015; Raizah *et al.*, 2018), the enclosure is a channel shape enclosure. The free convection heat transfer of non-Newtonian fluids in the axis-symmetric enclosures has been extensively overlooked in the literature. The free convection in 2D-axis symmetric enclosures can be fundamentally different from channel cavities due to the gradual increase of the cavity volume by the increase of axial distance. In the present study, the free convection behavior of a pseudoplastic-non-Newtonian fluid in a cylindrical enclosure partially filled by a layer of a porous medium is addressed for the first time. The study aims to address the following fundamental questions:

Q1. What is the effect of Rayleigh number on the flow field and temperature distribution of a pseudoplastic non-Newtonian fluid?

Q2. How the increase of pseudoplastic non-Newtonian affects the heat transfer and the temperature distribution in a cylindrical cavity?

Q3. What is the effect of a layer of highly conductive metal foam on the thermal behavior of a cylindrical enclosure?

To answer these questions, a model of flow and heat transfer in the cylindrical enclose is introduced in the next section.

2. Geometric and mathematical models

2.1 Physic of the problem

The cylindrical enclosure-space between two vertical pipes is filled with a non-Newtonian liquid. The model is two coaxial pipes, r_i and r_o, height L. A schematic view of the physical model, coordinate system, and boundary conditions are shown in Figure 1. Figure 1(a) illustrates the 3 D view of the model and Figure 1(b) and (c) depicts the side view and top view of the cylindrical cavity. The inner pipe is hot at the constant temperature of T_h, and the outer pipe is cold at the constant temperature of T_c. There is a layer of porous medium with the thickness of D over the hot pipe. The bottom and top geometry of the enclosure are adiabatic, $\partial T/\partial z = 0$, where T is the temperature. The flow and heat transfer are assumed axisymmetric and unsteady. Due to the buoyancy force, there is a laminar natural convection flow and heat transfer in the enclosure. The buoyancy effects are modeled using Boussinesq approximation. Preparing and cooking ketchup for food is a good example of the application of the present problem. If the sauce is inside the porous chamber, the heat transfer is better transmitted, and the sauce experiences a more uniform heat.

2.2 Governing equations

The governing equations in two-dimensional cylindrical coordinates (r,z) for continuity, laminar flow, and heat transfer in solid and liquid in the unsteady can be introduced as follows:

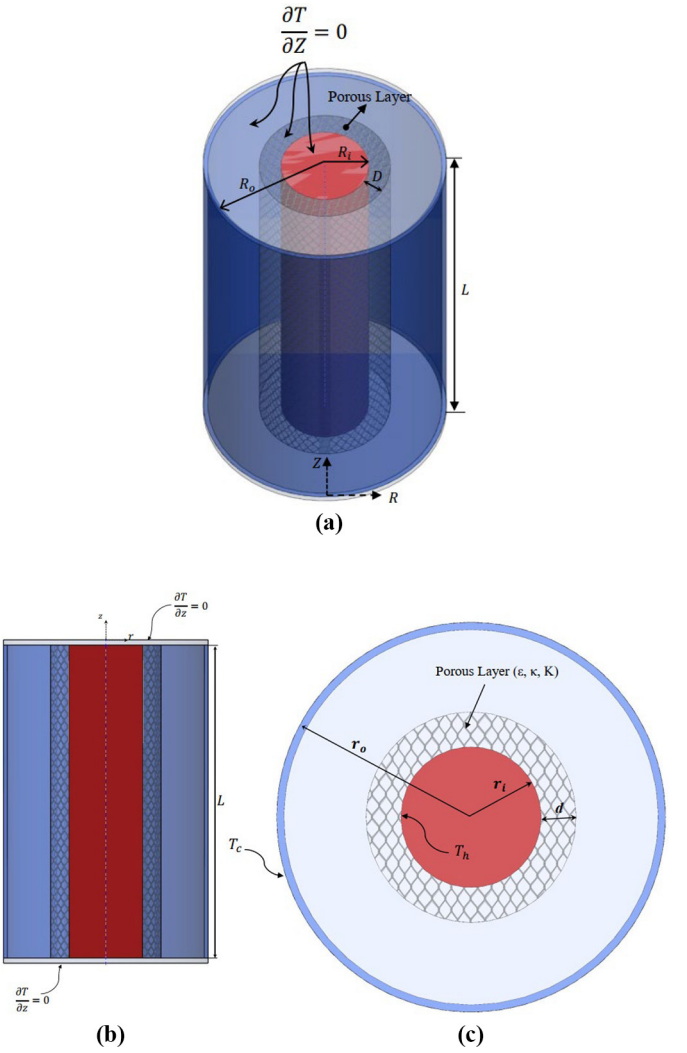

Figure 1.
Schematic representation of the physical problem (a) 2 D view; (b) 2 D view with boundary conditions; (c) 3 D view

Continuity equation:

$$\rho_f \nabla^* . (\overrightarrow{u}) = 0 \tag{1}$$

where $\overrightarrow{u}$ is the vector of velocity.

Momentum equation:

$$\frac{\rho_f}{\varepsilon}\frac{\partial \overrightarrow{u}}{\partial t} + \frac{\rho_f}{\varepsilon^2}(\overrightarrow{u}.\nabla^*)\overrightarrow{u} = \nabla^*\left[-pI + \frac{\mu_f}{\varepsilon}(\nabla \overrightarrow{u}) + (\nabla \overrightarrow{u})^T\right] - \frac{\mu_f}{\kappa}\overrightarrow{u} + \rho_f \overrightarrow{g}\beta_f \Delta T \tag{2}$$

in which ρ, ε, t, p, β, I and $\overrightarrow{g}$ are, respectively, density of the base fluid, porosity, time, pressure, permeability, thermal expansion coefficient, identity matrix and Gravity. Here, $\overrightarrow{u}$ is the velocity vector, and its components are u and v in r and z directions, respectively. The non-Newtonian dynamic viscosity is denoted by μ. To consider the non-Newtonian behavior of the fluid, the Power-law is used, based on this model can be written (Parmentier *et al.*, 1976; Panda and Chhabra, 2010; Sheela-Francisca *et al.*, 2012):

$$\mu_f(\dot{\gamma}) = m\mu_a \rightarrow \begin{cases} \mu_a = (\dot{\gamma})^{n-1} \\ \dot{\gamma} = \max\left(\sqrt{[D'] : [D']}, \dot{\gamma}_{\min}\right) \\ D' = \frac{1}{2}\left(\nabla \rightarrow u + (\nabla \rightarrow u)^T\right) \end{cases} \tag{3}$$

where μ_a is an apparent viscosity, $\dot{\gamma}$ is shear rate, $[D']$ is Strain rate tensor in fluid, $\nabla\overrightarrow{u}$ is velocity gradient tensor, m is a consistency index for non-Newtonian viscosity, and n is called power-law index the deviation of n from unity indicates the degree of deviation from Newtonian behavior, that is <1 for pseudoplastic, = 1 for Newtonian, and >1 for dilatant fluids. Pseudoplastic fluids are characterized by an apparent viscosity, which decreases with increasing shear rate.

Energy equation:

$$(\rho c_p)_{eff}\frac{\partial T}{\partial t} + (\rho c_p)_f \overrightarrow{u}.\nabla^* T = \nabla^*.\left(k_{eff}\nabla^* T\right) \tag{4}$$

where (Gao and Chen, 2011; Nield and Bejan, 2013):

$$(\rho c_p)_{eff} = (1-\varepsilon)(\rho c_p)_p + \varepsilon(\rho c_p)_f \tag{5}$$

$$k_{eff} = (1-\varepsilon)k_p + \varepsilon k_f \tag{6}$$

Here, T is the temperature, C_p is the heat capacity at constant pressure, k_{eff} is the effective thermal conductivity coefficient of the porous matrix. The subscripts of *eff*, p and f denote the effective properties, the porous medium and non-Newtonian fluid, respectively. The superscript * represents the dimensional variables.

According to problem definition in Figure 1, the corresponding boundary conditions for equations (1), (2) and (4) are:

$$r = r_i, z, t \rightarrow \overrightarrow{u} = 0, T = T_h \tag{7}$$

$$r = r_o, z, t \rightarrow \overrightarrow{u} = 0, T = T_c \tag{8}$$

$$r, z = 0, t \rightarrow \overrightarrow{u} = 0, \frac{\partial T}{\partial z} = 0 \tag{9}$$

$$r, z = L, t \rightarrow \vec{u} = 0, \frac{\partial T}{\partial z} = 0 \tag{10}$$

The initial condition of the problem is also defined as:

$$r, z, t = 0 \rightarrow \vec{u} = 0, T = T_0 \tag{11}$$

where in the present study it is assumed that the initial temperature is the same as the fusion temperature as $T_0 = T_c$. The following dimensionless variables are used to transform the governing equations into a non-dimensional form:

$$R_i = \frac{r_i}{L}, R_o = \frac{r_o}{L}, AR = \frac{L}{r_o - r_i}, Z = \frac{z}{L}, \vec{U} = \frac{\vec{u}L}{\alpha_f}, \theta = \frac{T - T_c}{T_h - T_c}, \tau = \frac{t\alpha_f}{L^2}, P = \frac{pL^2}{\rho_f \alpha_f^2},$$
$$\Pr = \frac{m}{\rho_f}\frac{\alpha_f^{n-2}}{L^{2n-2}}, Ra = \frac{\rho_f g \beta_f (T_h - T_c) L^{2n+1}}{m\alpha_f^n}, Da = \frac{\kappa}{L^2}, \sigma = \frac{(\rho c_p)_p}{(\rho c_p)_f}, \zeta = \frac{k_p}{k_f} \tag{12}$$

where some of these parameters have also been used in the study of Cao and Faghri (1990) for analysis of natural convection of a Newtonian fluid in a cavity. In the above equations, AR, τ, σ, ζ, Pr, Ra and Da represent the aspect ratio, non-dimensional time, ratio of heat capacity, ratio of thermal conductivity, Prandtl number, Rayleigh number and Darcy number, respectively. Here α_f is the thermal diffusivity introduced as thermal diffusivity $(k_f/(\rho c_p)_f)$. It should be noted that the Prandtl number or Rayleigh number maybe not in a full non-dimensional form as a non-integer index of n is involved.

It is worth noticing that considering the non-Newtonian index of n, some of the introduced non-dimensional parameters may be not in full non-dimensional form. However, the multiplex of these parameters is in non-dimensional form. By introducing the above dimensionless dependent and independent variables in the governing equations (1), (2) and (4), the following non-dimensional equations are obtained:

$$\rho_f(\nabla.\vec{U}) = 0 \tag{13}$$

$$\frac{1}{\varepsilon}\frac{\partial \vec{U}}{\partial t} + \frac{1}{\varepsilon^2}.(\vec{U}.\nabla)\vec{U} = \nabla.\left[-Pl + \frac{\Pr \dot{G}^{n-1}}{\varepsilon}(\nabla\vec{U}) + (\nabla\vec{U})^T\right] - \frac{\Pr}{Da}\dot{G}^{n-1}\vec{U} + \Pr\, Ra\theta_z \tag{14}$$

$$(\varepsilon + \sigma(1-\varepsilon))\frac{\partial \theta}{\partial \tau} + (\vec{U}.\nabla\theta) = (\varepsilon + \xi(1-\varepsilon))(\nabla.\nabla\theta) \tag{15}$$

The boundary conditions are also transformed into the following non-dimensional form:

$$R = R_i, Z, \tau \rightarrow \vec{U} = 0, \theta = 1 \tag{16}$$

$$R = R_o, Z, \tau \rightarrow \vec{U} = 0, \theta = 0 \tag{17}$$

$$R, Z = 0, \tau \rightarrow \vec{U} = 0, \frac{\partial \theta}{\partial Z} = 0 \tag{18}$$

$$R, Z = 1, \tau \rightarrow \vec{U} = 0, \frac{\partial \theta}{\partial Z} = 0 \tag{19}$$

$$R, Z, \tau = 0 \rightarrow \vec{U} = 0, \theta_0 = \frac{T_0 - T_c}{T_h - T_c} = 0 \tag{20}$$

It is worth noticing that in the above equation, the effect of cylindrical coordinate system and the cylindrical elements is also taken into account.The heat transfer at the surface of the hot wall, is defined using the energy balance at the surface as $h(T_h - T_c) = -k_{eff}\frac{\partial T}{\partial r})_{r=r_i}$. Using the non-dimensional variables of equation (12), the local Nusselt number can be rewritten as:

$$Nu_Z = \frac{hZ}{k_{eff}} = \frac{\partial \theta}{\partial R}\Bigg)_{R=R_i} \tag{21}$$

where the average Nusselt number can be evaluates as:

$$Nu_L = \int_o^1 Nu_Z dZ \tag{22}$$

3. Numerical method

The finite element method is employed to solve the partial differential equations introduced in the governing equations of equations (14)-(16) along with the boundary conditions of equations (17)-(22). Following the standard finite element method, the governing equations are written in the weak form. The boundary equations for the velocities and isothermal walls are Dirichlet boundary conditions; hence, Lagrange multiplier is employed. The momentum and continuity equations are discretized and solved by constricting algebraic equations over a structured grid. The first-order discretization is used for the heat equation. The heat and momentum equations are solved as fully coupled equations. More details about the finite element method can be found in recent study regarding the finite element solution of non-Newtonian fluids by Castillo and Codina (2014) and the textbooks by Huang *et al.* (2012), Nithiarasu *et al.* (2016), and Pepper and Heinrich (2017).

A time-dependent automatic time-stepping approach based on the backward differentiation formulas (BDF) with minimum BDF order of 1 and maximum BDF order of 2 and free time steps is used (De Los Reyes and González Andrade, 2012). Newton method with the damping factor of 0.9 along with the PARDISO solver (Schenk and Gärtner, 2004; Wriggers, 2008) are used to residual equations. The computations are repeated until the error of computation reaches below 10^{-6} in each time step. The results were reported for a steady-state solution. The steady-state solution was obtained after a sufficiently long time.

3.1 Grid check

The adequate size of the grid was found by testing several structured grid sizes of $N_z \times N_r$. The profiles of non-dimensional vertical velocity and non-dimensional temperature along the centerline of the cylindrical cavity, $Z = 0.5$, are monitored and reported for the selected grid sizes. Figure 2 depicts a sample of the structured grid with the size of 150×150. Figure 3 shows the vertical velocity (U_z) and temperature profile (θ) along R at $Z = 0.5$ when aspect

ratio $AR = 1$, $R_i = 0.4$, $D = 0.1$, $n = 0.5$, $Pr = 60$, $Da = 10^{-4}$ and $Ra = 10^4$. The specific heat ratio σ and the thermal conductivity ratio ζ are adopted as $\sigma = 30.68$ and $\zeta = 1000$.

The results of Figure 3 show that the variation of the results by the change in the size of the grid is very small. To determine the optimal number of meshes in the grid for different directions, the dimensionless axial velocity (U_Z), and the dimensionless temperature (θ) were compared for three different grids at mid-height of the annulus ($Z = 0.5$). The grid size of 150×150 can produce adequate accuracy for most engineering applications and graphical illustrations. Hence, the grid size 150×150 is selected for future calculations in this study.

3.2 Validation of computation

The numeric results of the present work are compared with the literature results in several cases. As a first comparison, the study of Basak *et al.* (2009) adopted. In Basak *et al.* (2009), the natural convection flow and heat transfer in a trapezoidal enclosure were explored. They employed the Galerkin finite element method to solve the governing differential equations for continuity, momentum, and energy in the enclosure. Considering a 2D Cartesian coordinate system and heating from bottom, and assuming a Newtonian fluid, the results of the present study can be compared with the study of Basak *et al.* (2009). The comparison is depicted in Figure 4. Figure 4 illustrates the variation of local Nusselt number at the hot wall when $Pr = 7.2$, $Da = 10^{-3}$ and $Ra = 10^6$. As seen, the results show a very good agreement between the results of the present numerical solution and the literature results.

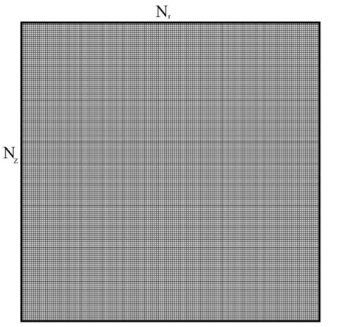

Figure 2.
An adapted structured grid on the case

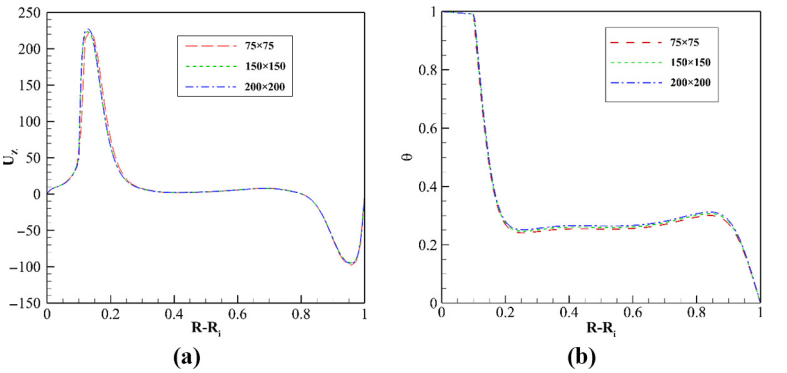

Figure 3.
Profiles of dimensionless axial velocity (a), and dimensionless temperature; (b) for different grids ($AR = 1$, $R_i = 0.4$, $D = 0.1$ and $n = 0.5$, $Pr = 60$, $Da = 10^{-4}$, $Ra = 10^4$)

As another validation, the results of the current work are compared with (Kakarantzas *et al.*, 2017). Kakarantzas *et al.* (2017) addressed the natural convection flow and heat transfer of MHD liquid metal in an enclosure space between two coaxial vertical cylinders. The liquid metal was subject to a uniform magnetic field which was applied horizontally and the enclosure walls were electrically insulated. In Kakarantzas *et al.* (2017) the vertical walls are isotherm, and the outer cylinder is hotter than the inner cylinder. Assuming a Newtonian flow, considering a zero magnetic field ($Ha = 0$), the results of the present study are compared to the benchmark study of (Kakarantzas *et al.*, 2017) when $Ra = 10^5$, $Pr = 0.0321$. Figure 5 illustrates an acceptable agreement between the results of the present study and the results of Kakarantzas *et al.* (2017).

Matin and Khan (2013) addressed the steady-state natural convection flow and heat transfer of a power-law fluid in the space between two concentric horizontal cylinders. The cylinders were isothermal with different temperatures. Figure 6 compares the Nusselt number obtained in the current work and those reported in (Matin and Khan, 2013) when $Pr = 10$ and $Ra = 10^3$. The results are plotted for the various value of non-Newtonian index n.

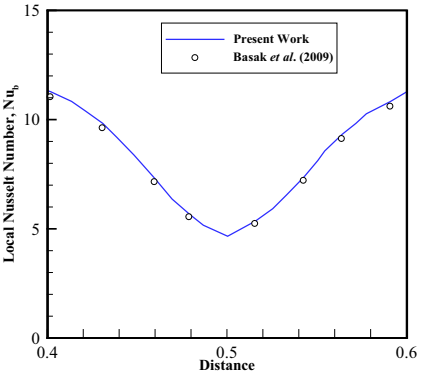

Figure 4.
Variation of local Nusselt number at the hot wall in the presence of uniform heating

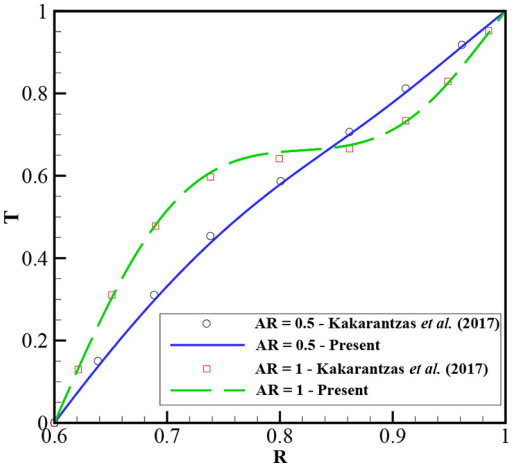

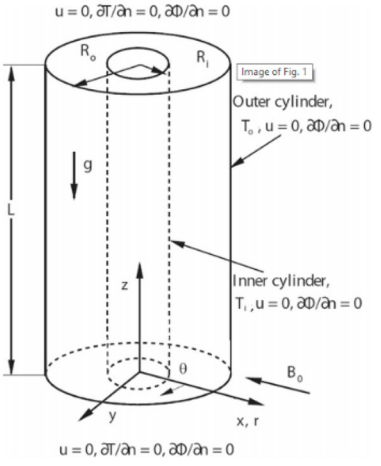

Figure 5.
A comparison between the radial distribution of temperature for $Ha = 0$, $AR = 0.5$, and $AR = 1$ and the current results when $R_o - R_i = 0.6$ at middle height

Figure 6 also indicates an excellent agreement between the results of the present study and the literature results.

4. Results and discussion

4.1 Effect of Rayleigh number

The default value of the non-dimensional parameters are selected as $AR = 1$, $R_i = 0.4$, $\varepsilon = 0.2$, $Ra = 10^4$, $Pr = 60$, $Da = 10^{-4}$, $D = 0.1$, $\sigma = 30.68$, $\zeta = 1000$ and $n = 0.9$. The high value of Pr corresponds to paraffin materials. These non-dimensional parameters will be used to represent the results; otherwise, the value of the non-dimensional parameter will be stated.

Figure 7 shows the streamlines and the temperature profiles in the cavity for various values of Rayleigh number. The dashed line shows the thickness of the porous layer D. The red dash line shows the region of the porous medium. When the Rayleigh number is small, there is no or only one streamline in the porous space. The velocity and fluid movements are very limited in the porous space due to the high hydraulic resistance of the porous medium. By the increase of Ra, the buoyancy forces get stronger, and hence, the number of streamlines in the enclosure increases. Considering Ra number, defined as the ratio of Buoyancy to diffusion, for low values of Ra, the effects of buoyancy are low, convective heat transfer is weak, and the isothermal lines are nearly vertical following the conduction heat transfer. By the increase of Ra, the isothermal lines assume a wave shape, and the convective heat transfer gets stronger. A $Ra = 10^6$, the isotherms are nearly horizontal. This is due to the strong flows of the fluid at the top and bottom of the cavity. At the top of the cavity, the fluid is hot, and at the bottom, the fluid is cold. Therefore, the dominant temperature gradient is in a vertical direction from top to bottom.

As mentioned, by the increase of Ra to 10^6, the buoyancy force gets stronger. The streamlines enter effectively into the porous region, and they also induce a temperature gradient at the porous medium. Indeed, for the Rayleigh numbers about 10^5 or lower, the resistance in the clear-region liquid layer was the dominant resistance mechanism in the cavity. Therefore, the temperature gradient in the porous medium was almost negligible due to the high value of the effective thermal conductivity of the porous medium. By the increase of Rayleigh number to 10^6, the thermal resistance of the liquid layer is comparable with the resistance of heat diffusion in the porous layer, and hence, the temperature gradients in the porous region boost. Thus, the contours of isotherm enter into the porous region. In this case, the isothermal lines of 0.85 and 0.95 are inclined into the porous region.

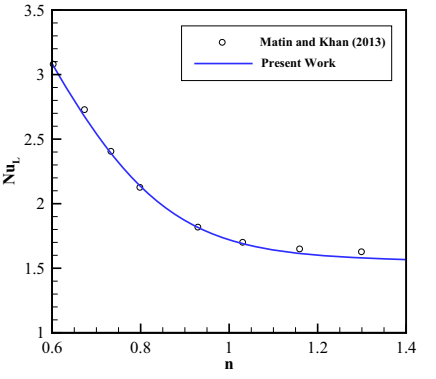

Figure 6.
A comparison between the results of present work and the study of Matin and Khan (2013)

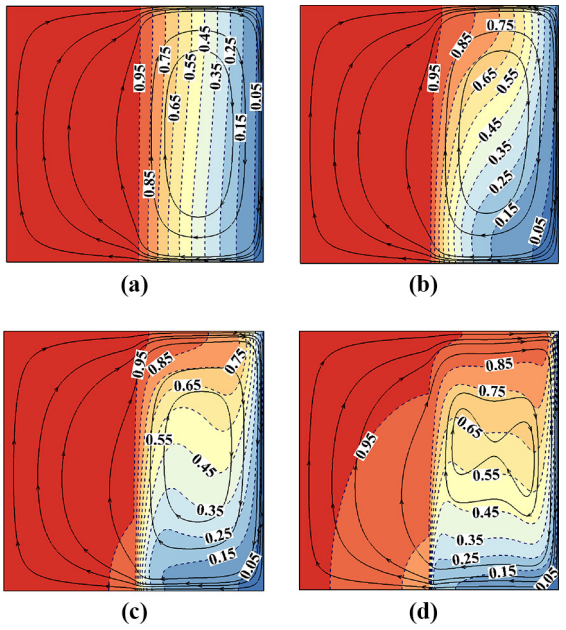

Figure 7.
Streamlines and temperature contour for D = 0.5 and different Rayleigh number when (a) $Ra = 10^3$; (b) $Ra = 10^4$; (c) $Ra = 10^5$ and (d) $Ra = 10^6$

4.2 Effect of non-Newtonian index

Figure 8 illustrates the streamlines and temperature contours for various values of non-Newtonian index n. As seen, the variation of the non-Newtonian index n notably changes the streamlines and temperature contours in the cavity. In the case of $n = 0.9$ which the fluid is almost a Newtonian fluid, the streamlines are circular. The symmetry between the isotherms at the cold and hot walls can be observed. By the decrease of n, in which the fluid exhibits stronger non-Newtonian effects, the streamlines lose their circular shape and deflect toward the upper wall of the cavity. As seen, in the case of $n = 0.5$, there is no symmetry in the streamlines. This is because of the cylindrical shape of the enclosure. In a cylindrical enclosure by the increase of the distance from the axis, the premiere of the cavity increases, and hence, the velocity and velocity gradients drop. In the case of strongly non-Newtonian fluid, Figure 8(a), in which the dynamic viscosity is a strong function of shear rate (velocity gradients), the symmetrical shape of the streamlines lost. Following the significant change in the velocity profiles and streamlines, the temperature distribution in the cavity is also affected. As seen in Figure 8(a), the temperature contours are concentrated at the top-left region of the cavity where the streamlines are also concentrated.

The local Nusselt number along the hot wall is plotted in Figure 9 for the various value of non-Newtonian index n. This figure reveals that increasing the non-Newtonian effect of the fluid (decreases of n) significantly increases the Nusselt number. As it was observed in streamlines and temperature contours of Figure 8, in the case of strong non-Newtonian pseudoplastic fluid, i.e. $n = 0.5$, the increase of the shear rate reduces the apparent dynamic viscosity, and hence, the velocity of the fluid increases. The increase of the fluid velocity consequently enhances the local Nusselt number and heat transfer in the cavity.

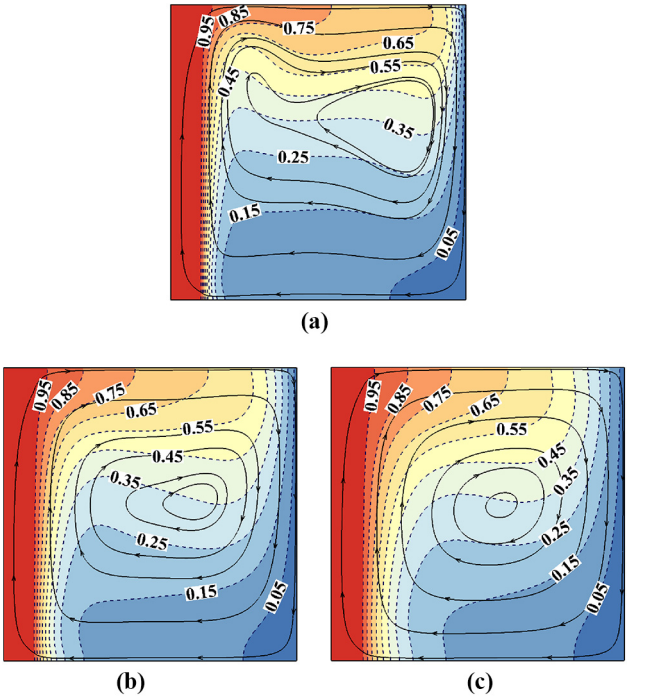

Figure 8.
Streamline and temperature contours for (a) $n = 0.5$; (b) $n = 0.7$ and (c) $n = 0.9$

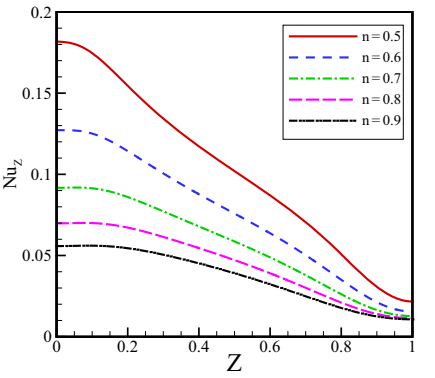

Figure 9.
Variation of the Nusselt number along the wall

4.3 Effect of thickness of porous layer

Figure 10 shows the streamlines and the temperature profiles for various thicknesses of the porous layer, D. The results are plotted for a very low porous thickness ($D = 0.05$), the thickness of the porous layer lays up to the middle of the cavity ($D = 0.5$), and the porous layer almost filled all of the cavity $D = 0.9$. The temperature profiles show that in all of the cases, the temperature in the porous layer is almost uniform and high. This is due to the high value of the effective thermal conductivity of the porous medium. Hence, in the porous

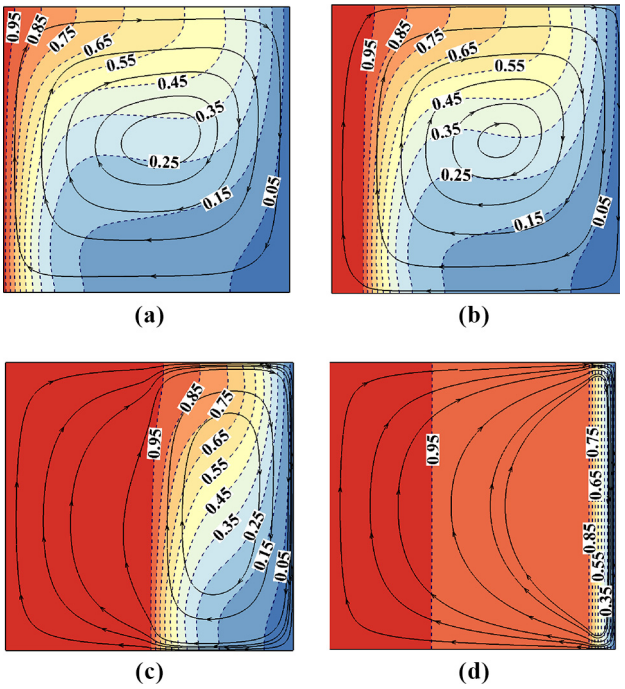

Figure 10.
Streamlines and the temperature profiles for (a) $D = 0$ (No porous layer); (b) $D = 0.1$; (c) D = 0.5 and (d) $D = 0.9$

layer, the dominant mechanism of heat transfer is diffusion, and the thermal resistance of the porous medium is much lower than that of the clear region. Thus, no significant temperature gradients can be seen in the porous layer. The streamlines show when the porous layer is narrow, and the clear flow is wide, the fluid can easily circulate in the clear region. By the increase of the porous layer to $D = 0.9$, the clear flow region is narrow, and the fluid is under the significant influence of the no-slip at the boundaries and the porous medium. In this case, the hydraulic resistance of the clear flow is comparable with the porous medium, and the streamlines enter into the porous medium. However, the distance between the streamlines is high and the flow velocities are very low. The attention to isotherms in the cases of $D = 0.1$ and $D = 0.5$ shows that the isotherms are under the influent of the flow convection, but by the increase of D, this influence decreases. In the case of $D = 0.9$, a dominant thermal diffusion in both clear flow and solid region can be seen.

Figure 11 shows the temperature profile at different horizontal sections of the cylinder when $D = 0.5$. Figure 11(a) and (b) depict the results for $Ra = 10^4$ and $Ra = 10^5$, respectively. As shown in the figure, isothermal lines are so close together in the porous region, while in the clear flow region, the difference between the temperature profiles is obvious. The comparison of the temperature profiles in Figure 11(a) and (b) in the porous region shows that by the increase of Rayleigh number the slope of the temperature profiles at the porous region increases. This is due to the reduction of the thermal resistance of the clear flow region by the increase of Rayleigh number.

The average Nusselt number as a function of the porous layer thickness (D) is plotted in Figure 12. This figure shows the increase of the porous layer slightly increases the heat transfer rate in the enclosure as the thickness of the porous layer increases when the

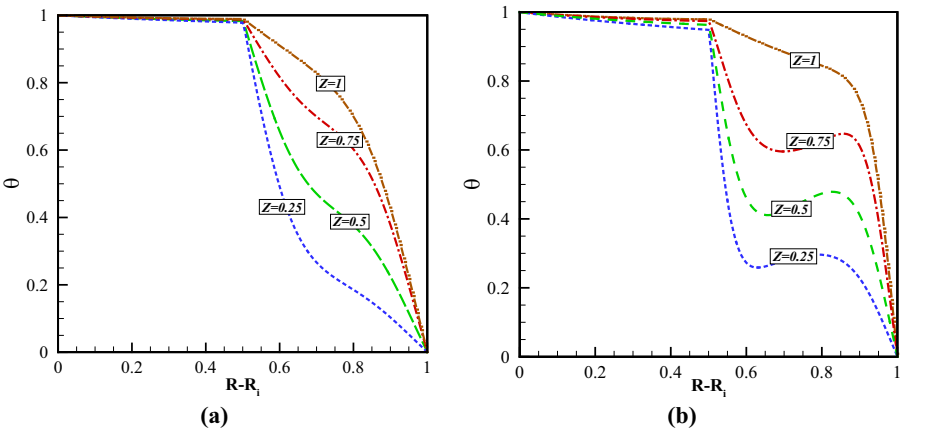

Figure 11.
Temperature profile at different horizontal section of the cylinder for different (a) $Ra = 10^4$; (b) $Ra = 10^5$

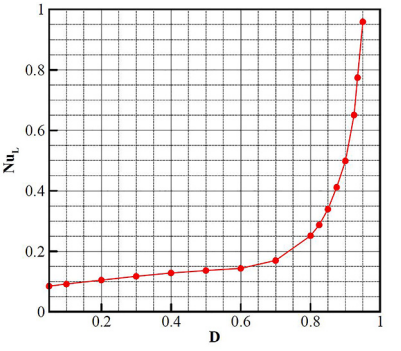

Figure 12.
The Nusselt number for different thicknesses of the porous medium

thickness of the porous layer is low, $D < 0.6$. This is since the increase of the porous thickness suppresses the convection heat transfer in the clear region and increases the thermal resistance of this region. However, as the temperature in the porous region is uniformly close to the temperature of the hot wall, in fact, the increase of the thickness of the porous region reduces the distance between the hot wall and the cold wall which tends to enhance the heat transfer rate. By the competition of these two opposite effects, the Nusselt number increases smoothly up to $D = 0.6$. By further grow of D, the distance between the hot wall and the cold wall reduces while as it was observed in Figure 10(c) the convection flow also enters into the porous region and further decreases the thermal resistance of the clear flow by mixing of the fluid with the hot flow inside the porous region. As a result, the Nusselt number increases gradually.

5. Conclusion

In this study, flow and heat transfer of a non-Newtonian fluid in a cylindrical vertical enclosure partially filled with a layer of porous medium is investigated numerically. The finite element method was employed to solve the governing equations. The grid

independence of the results and validations are performed. The effect of the non-Newtonian power index (n) and the thickness of the porous layer (D) on the natural convection flow and heat transfer were investigated. The outcomes can be summarized as follows:

- Local Nu number is maximum at the lower corner of the internal cylinder and minimum at the upper corner. For a larger Rayleigh number, temperature gradients are larger and are confined in a small area near the vertical walls.
- The decrease of the power index n reduces the symmetry of the streamlines and velocity distributions in the cavity. This is due to the geometry of the cylindrical cavity and the axis-symmetric elements. Local Nu number is maximum at the lower corner of the internal cylinder and minimum at the upper corner. For a larger Rayleigh number, temperature gradients are larger and are confined in a small area near the vertical walls. The increase of pseudoplastic plastic behavior of the fluid in the cavity (decrease of n) enhances both local Nusselt number and the average Nusselt number in the cavity.
- The increase of the thickness of the porous layer enhances the heat transfer in the cavity. When the thickness of the porous layer is low, $D < 0.6$, the enhancement in the heat transfer due to the presence of the porous layer is low. In the case of a porous layer with a higher thickness ($D > 0.6$), a notable enhancement in the average Nusselt number can be observed. By increase of the porous layer from $D = 0.6$ to $D = 0.8$, the average Nusselt number improved by 1.6 fold from $Nu_L = 0.15$ to $Nu_L = 0.25$.

The geometry of a cylindrical vertical cavity is of interest for its various practical applications in the storage tanks and heat exchangers. The important point about the cylindrical cavity is the fact that by an increase of distance from the axis, the perimeter of the cavity in the 3D model increases. Therefore, considering the continuity equation, the natural convection flow and shear rates next to the inner wall of the cavity are stronger than that of the outer wall of the cavity. Hence, the apparent viscosity for the fluid next to the inner wall, and the outer wall of the cavity are not similar. This leads to a non-symmetric distribution of velocity and temperature profiles in the cavity. There are many unexplored aspects of natural convection in the cylindrical cavities with non-Newtonian behavior such as a cavity with partially heated wall and heating from below which can be subject of future studies.

References

Alsabery, A.I., Hussain, S.H., Saleh, H. and Hashim, I. (2015), "Inclination angle effect on natural convection in a square cavity partially filled with non-Newtonian fluids layer", *AIP Conference Proceedings*, *AIP Publishing*, p. 60007.

Alsabery, A., Chamkha, A., Hashim, I. and Siddheshwar, P. (2017a), "Effects of nonuniform heating and wall conduction on natural convection in a square porous cavity using LTNE model", *Journal of Heat Transfer*, Vol. 139 No. 12, p. 122008.

Alsabery, A.I., Chamkha, A.J., Saleh, H. and Hashim, I. (2017b), "Transient natural convective heat transfer in a trapezoidal cavity filled with non-Newtonian nanofluid with sinusoidal boundary conditions on both sidewalls", *Powder Technology*, Vol. 308, pp. 214-234.

Alsabery, A.I., Mohebbi, R., Chamkha, A.J. and Hashim, I. (2019), "Effect of local thermal non-equilibrium model on natural convection in a nanofluid-filled wavy-walled porous cavity containing inner solid cylinder", *Chemical Engineering Science*, Vol. 201.

Alsabery, A.I., Tayebi, T., Chamkha, A.J. and Hashim, I. (2018), "Effect of rotating solid cylinder on entropy generation and convective heat transfer in a wavy porous cavity heated from below", *International Communications in Heat and Mass Transfer*, Vol. 95, pp. 197-209.

Asl, A.K., Hossainpour, S., Rashidi, M., Sheremet, M. and Yang, Z. (2019), "Comprehensive investigation of solid and porous fins influence on natural convection in an inclined rectangular enclosure", *International Journal of Heat and Mass Transfer*, Vol. 133, pp. 729-744.

Astanina, M.S., Sheremet, M. and Umavathi, C.J. (2019), "Unsteady natural convection in a partially porous cavity having a heat-generating source using local thermal non-equilibrium model", *International Journal of Numerical Methods for Heat and Fluid Flow*, Vol. 29 No. 6, pp. 1902-1919.

Basak, T., Roy, S., Singh, A. and Balakrishnan, A. (2009), "Natural convection flows in porous trapezoidal enclosures with various inclination angles", *International Journal of Heat and Mass Transfer*, Vol. 52 Nos 19/20, pp. 4612-4623.

Biswal, U., Chakraverty, S. and Ojha, B.K. (2019), "Natural convection of non-Newtonian nanofluid flow between two vertical parallel plates", *International Journal of Numerical Methods for Heat and Fluid Flow*, Vol. 29 No. 6, pp. 1984-2008.

Cao, Y. and Faghri, A. (1990), "A numerical analysis of phase-change problems including natural convection", *Journal of Heat Transfer*, Vol. 112 No. 3, pp. 812-816.

Castillo, E. and Codina, R. (2014), "Stabilized stress–velocity–pressure finite element formulations of the navier–stokes problem for fluids with non-linear viscosity", *Computer Methods in Applied Mechanics and Engineering*, Vol. 279, pp. 554-578.

Chamkha, A., Rashad, A., Mansour, M., Armaghani, T. and Ghalambaz, M. (2017), "Effects of heat sink and source and entropy generation on MHD mixed convection of a Cu-water nanofluid in a lid-driven square porous enclosure with partial slip", *Physics of Fluids*, Vol. 29 No. 5, p. 52001.

Cheng, C.Y. (2009), "Natural convection heat transfer of non-Newtonian fluids in porous media from a vertical cone under mixed thermal boundary conditions", *International Communications in Heat and Mass Transfer*, Vol. 36 No. 7, pp. 693-697.

Chhabra, R.P. and Richardson, J.F. (1999), *Non-Newtonian Flow in the Process Industries: fundamentals and Engineering Applications*, Butterworth-Heinemann.

De Los Reyes, J.C. and González Andrade, S. (2012), "A combined BDF-semismooth newton approach for time-dependent Bingham flow", *Numerical Methods for Partial Differential Equations*, Vol. 28 No. 3, pp. 834-860.

Dogonchi, A., Sheremet, M., Ganji, D. and Pop, I. (2019), "Free convection of copper–water nanofluid in a porous gap between hot rectangular cylinder and cold circular cylinder under the effect of inclined magnetic field", *Journal of Thermal Analysis and Calorimetry*, Vol. 135 No. 2, pp. 1171-1184.

Gao, D. and Chen, Z. (2011), "Lattice Boltzmann simulation of natural convection dominated melting in a rectangular cavity filled with porous media", *International Journal of Thermal Sciences*, Vol. 50 No. 4, pp. 493-501.

Harab, B.A., Calisir, T. and Baskaya, S. (2019), "Numerical investigation of transient natural convection heat transfer of non-Newtonian nanofluids between eccentric annulus", *Arabian Journal for Science and Engineering*, Vol. 44 No. 6, pp. 5631-5646.

Huang, H.C., Li, Z.H. and Usmani, A.S. (2012), *Finite Element Analysis of non-Newtonian Flow: theory and Software*, Springer Science and Business Media.

Jahanbakhshi, A., Nadooshan, A.A. and Bayareh, M. (2018), "Magnetic field effects on natural convection flow of a non-Newtonian fluid in an L-shaped enclosure", *Journal of Thermal Analysis and Calorimetry*, Vol. 133 No. 3, pp. 1407-1416.

Kairi, R.R. and Murthy, P.V.S.N. (2009), "Effect of melting and thermo-diffusion on natural convection heat mass transfer in a non-Newtonian fluid saturated non-Darcy porous medium", *The Open Transport Phenomena Journal*, Vol. 1 No. 1, pp. 7-14.

Kairi, R.R. and Murthy, P.V.S.N. (2012), "Effect of melting on mixed convection heat and mass transfer in a non-Newtonian fluid saturated non-Darcy porous medium", *Journal of Heat Transfer*, Vol. 134 No. 4, p. 42601.

Kakarantzas, S., Benos, L.T., Sarris, I., Knaepen, B., Grecos, A. and Vlachos, N. (2017), "MHD liquid metal flow and heat transfer between vertical coaxial cylinders under horizontal magnetic field", *International Journal of Heat and Fluid Flow*, Vol. 65, pp. 342-351.

Kefayati, G. (2016a), "Heat transfer and entropy generation of natural convection on non-Newtonian nanofluids in a porous cavity", *Powder Technology*, Vol. 299, pp. 127-149.

Kefayati, G.R. (2016b), "Simulation of double diffusive natural convection and entropy generation of power-law fluids in an inclined porous cavity with soret and dufour effects (part I: Entropy generation)", *International Journal of Heat and Mass Transfer*, Vol. 94, pp. 539-581.

Kefayati, G.R. (2016c), "Simulation of double diffusive natural convection and entropy generation of power-law fluids in an inclined porous cavity with soret and dufour effects (part II: Entropy generation)", *International Journal of Heat and Mass Transfer*, Vol. 94, pp. 582-624.

Kefayati, G.R. (2019), "Lattice boltzmann simulation of double-diffusive natural convection of viscoplastic fluids in a porous cavity", *Physics of Fluids*, Vol. 31 No. 1, p. 013105.

Loenko, D.S., Shenoy, A. and Sheremet, M.A. (2019), "Natural convection of Non-Newtonian Power-Law fluid in a square cavity with a Heat-Generating element", *Energies*, Vol. 12 No. 11, p. 2149.

Matin, M.H. and Khan, W.A. (2013), "Laminar natural convection of non-Newtonian power-law fluids between concentric circular cylinders", *International Communications in Heat and Mass Transfer*, Vol. 43, pp. 112-121.

Mehryan, S., Sheremet, M.A., Soltani, M. and Izadi, M. (2019), "Natural convection of magnetic hybrid nanofluid inside a double-porous medium using two-equation energy model", *Journal of Molecular Liquids*, Vol. 277, pp. 959-970.

Miroshnichenko, I.V., Sheremet, M.A., Oztop, H.F. and Abu-Hamdeh, N. (2018), "Natural convection of alumina-water nanofluid in an open cavity having multiple porous layers", *International Journal of Heat and Mass Transfer*, Vol. 125, pp. 648-657.

Mohebbi, R., Delouei, A.A., Jamali, A., Izadi, M. and Mohamad, A.A. (2019), "Pore-scale simulation of non-Newtonian power-law fluid flow and forced convection in partially porous media: Thermal lattice boltzmann method", *Physica A: Statistical Mechanics and Its Applications*, Vol. 525, pp. 642-656.

Nield, D.A. and Bejan, A. (2013), *Convection in Porous Media*, Springer.

Nithiarasu, P., Lewis, R.W. and Seetharamu, K.N. (2016), *Fundamentals of the finite element method for heat and mass transfer*.

Panda, S.K. and Chhabra, R.P. (2010), "Laminar flow of power-law fluids past a rotating cylinder", *Journal of Non-Newtonian Fluid Mechanics*, Vol. 165 Nos 21/22, pp. 1442-1461.

Parmentier, E.M., Turcotte, D.L. and Torrance, K.E. (1976), "Studies of finite amplitude non-Newtonian thermal convection with application to convection in the earth's mantle", *Journal of Geophysical Research*, Vol. 81 No. 11, pp. 1839-1846.

Pepper, D.W. and Heinrich, J.C. (2017), *The Finite Element Method: Basic Concepts and Applications with MATLAB, MAPLE, and COMSOL*, 3rd Edition, CRC Press, Boca Raton.

Pishkar, I., Ghasemi, B., Raisi, A. and Aminossadati, S.M. (2019), "Numerical study of unsteady natural convection heat transfer of Newtonian and non-Newtonian fluids in a square enclosure under oscillating heat flux", *Journal of Thermal Analysis and Calorimetry*, pp. 1-14, doi: 10.1007/s10973-019-08253-1.

Quarteroni, A., Tuveri, M. and Veneziani, A. (2000), "Computational vascular fluid dynamics: problems, models and methods", *Computing and Visualization in Science*, Vol. 2 No. 4, pp. 163-197.

Raizah, Z., Aly, A.M. and Ahmed, S.E. (2018), "Natural convection flow of a power-law non-Newtonian nanofluid in inclined open shallow cavities filled with porous media", *International Journal of Mechanical Sciences*, Vol. 140, pp. 376-393.

Schenk, O. and Gärtner, K. (2004), "Solving unsymmetric sparse systems of linear equations with PARDISO", *Future Generation Computer Systems*, Vol. 20 No. 3, pp. 475-487.

Sheela-Francisca, J., Tso, C.P., Hung, Y.M. and Rilling, D. (2012), "Heat transfer on asymmetric thermal viscous dissipative couette–poiseuille flow of pseudo-plastic fluids", *Journal of Non-Newtonian Fluid Mechanics*, Vol. 169, pp. 42-53.

Sheremet, M.A. (2012), "Laminar natural convection in an inclined cylindrical enclosure having finite thickness walls", *International Journal of Heat and Mass Transfer*, Vol. 55 Nos 13/14, pp. 3582-3600.

Sheremet, M.A. and Pop, I. (2018), "Effect of local heater size and position on natural convection in a tilted nanofluid porous cavity using LTNE and buongiorno's models", *Journal of Molecular Liquids*, Vol. 266, pp. 19-28.

Sheremet, M.A. and Trifonova, T.A. (2013), "Unsteady conjugate natural convection in a vertical cylinder partially filled with a porous medium", *Numerical Heat Transfer, Part A: Applications*, Vol. 64 No. 12, pp. 994-1015.

Sheremet, M.A. and Trifonova, T.A. (2014), "Unsteady conjugate natural convection in a vertical cylinder containing a horizontal porous layer: Darcy model and brinkman-extended Darcy model", *Transport in Porous Media*, Vol. 101 No. 3, pp. 437-463.

Siavashi, M. and Vamerzani, B.Z. (2016), "Numerical simulation of two-phase non-Newtonian polymer flooding in porous media to enhance oil recovery", *Modares Mechanical Engineering*, Vol. 16, pp. 297-307.

Sivasankaran, S., Alsabery, A. and Hashim, I. (2018), "Internal heat generation effect on transient natural convection in a nanofluid-saturated local thermal non-equilibrium porous inclined cavity", *Physica A: Statistical Mechanics and Its Applications*, Vol. 509, pp. 275-293.

Wriggers, P. (2008), *Nonlinear Finite Element Methods*, Springer Science and Business Media.

Corresponding author
Mohammad Ghalambaz can be contacted at: mohammad.ghalambaz@tdtu.edu.vn